Available online at www.sciencedirect.com
ScienceDirect
Applied Surface Science 253 (2007) 4085–4093
applied surface science
www.elsevier.com/locate/apsusc

The oxidation of calcium implanted titanium in water: A depth profiling study

D.A. Armitage [a,*], R. Mihoc [a], T.J. Tate [b], D.S. McPhail [c], R. Chater [c], J.A. Hobkirk [d], L. Shinawi [a,1], F.H. Jones [a,e]

[a] Division of Biomaterials and Tissue Engineering, UCL Eastman Dental Institute, University College London, 256, Gray's Inn Road, London WC1X 8LD, UK
[b] Department of Electrical and Electronic Engineering, Imperial College London, South Kensington Campus, London SW7 2AZ, UK
[c] Department of Materials, Imperial College London, Prince Consort, London SW7 2AZ, UK
[d] Division of Restorative Dental Sciences, UCL Eastman Dental Institute, University College London, 256, Gray's Inn Road, London WC1X 8LD, UK
[e] Department of Chemistry, University College London, Christopher Ingold Building, 20, Gordon Street, London WC1H 0AJ, UK

Received 10 May 2006; received in revised form 9 August 2006; accepted 5 September 2006
Available online 17 October 2006

Abstract

Ion implantation of calcium has been proposed previously as a route to bioactive titanium surfaces and has been shown to stimulate promising cell and tissue responses. While the precise reasons for this behaviour remain poorly understood, it is clear that the nature of the Ca implanted surface changes rapidly on exposure to body fluids. In order to understand the processes taking place more clearly, the current work examined the simple interaction of Ca implanted Ti with water. The surface chemistry and compositional changes within the sub-surface region of the modified Ti were examined. On immersion in water, the concentration of implanted Ca ions was found to decrease both at the surface and throughout the implanted region. At the same time, the sub-surface oxygen concentration was found to increase dramatically. Although Ca implantation into Ti results in a thicker oxide layer at the surface, it appears that this layer no longer affords the underlying Ti the same protection from further oxidation provided by the native oxide. By examining samples implanted with O, Ti or Ar it was possible to conclude that this was specific to Ca implantation and not a result of the ion implantation process itself.

Keywords: Ion implantation; Titanium; Calcium; Biomaterials; X-ray photoelectron spectroscopy; Secondary ion mass spectrometry

1. Introduction

Titanium is used extensively as a dental implant material and forms the basis of alloys employed elsewhere in the body. Modification of Ti by ion implantation has been of interest for some time, primarily as a method to enhance the corrosion resistance of the metal [1]. In addition, *in vivo* studies have revealed that implantation of calcium ions resulted in more new bone and greater bone-surface contact at early time periods [2,3]. Initial cell culture experiments *in vitro* provided no real explanation for this apparent enhancement of osseointegration; although Ca implantation appeared to have no detrimental effect on human derived bone cells in contact with the metal, neither viability, nor alkaline phosphatase activity were enhanced compared to non-implanted control Ti [4]. In more recent experiments [5–7], however, Ca implantation was found to have significant effects on the behaviour of bone cells (both primary cultures and cell lines). For example, in comparison with non-implanted Ti and Ti implanted with K or Ar, Ca–Ti inhibited cell attachment after short culture periods (4 h), but the cells that did adhere exhibited enhanced spreading and growth compared to control surfaces [5,6]. Notably, after 24 h of cell culture, the number of cells attached to the Ca–Ti surface was significantly increased compared to the control Ti [7].

The reasons for this behaviour have not been fully established. A number of factors are likely to be important.

* Corresponding author. Tel.: +44 20 7915 1090; fax: +44 20 7915 1227.
E-mail address: d.armitage@eastman.ucl.ac.uk (D.A. Armitage).
[1] Present address: Removable Prosthodontics Division, Faculty of Dentistry, King Abdul Aziz University, P.O. Box 80209, Jeddah 21589, Saudi Arabia.

0169-4332/$ – see front matter © 2006 Elsevier B.V. All rights reserved.
doi:10.1016/j.apsusc.2006.09.006

The surface chemistry following ion implantation will be different from that of the native Ti oxide, with a different surface energy and surface charge in solution. This may affect interactions with both inorganic ions and biomolecules in the solution. Dynamic processes may also occur, such as surface dissolution and ion release. In turn this may influence the local pH and ion concentrations in the vicinity of the surface, potentially affecting cellular activity.

The structure of the Ca–Ti surface has been examined in some detail [4,8–13]. It is well established that implantation of Ca into Ti results in the accelerated formation of calcium phosphates when immersed in simulated body fluids [4,12–14]. As calcium phosphates, especially hydroxyapatite (HA), have been exploited as bioactive materials, their apparently spontaneous formation at certain surfaces is of great interest [15]. However, the mechanisms of their formation remain poorly understood. Precipitation may depend on the availability of Ti–OH groups as nucleation sites on the surface [14,16], as indicated by increased OH concentrations measured on Ca–Ti compared to polished Ti [17]. Solution parameters such as local ion concentrations and pH are also important, however, and it has been suggested that the release of Ca ions from Ca–Ti may result in supersaturation with respect to calcium phosphate in the local environment of the surface, triggering spontaneous precipitation [14,16].

Ion release into certain solutions has been studied in detail, using Auger electron spectroscopy in combination with argon ion sputtering to obtain depth profiles of Ca implanted Ti [18,19]. The results showed that Ca was released into nitric acid or phosphate-citric acid buffers within 2 h of immersion. The acid environment was also found to result in thinning of the surface oxide. However, the acidity of the solutions used and the presence of other ions are likely to have influenced both the ion release and the surface chemistry following immersion.

Therefore, in order to better understand the mechanisms by which Ca ion implantation alters the behaviour of Ti surfaces, this study examined the surface and sub-surface composition of Ca–Ti before and after immersion in ultra-pure water. X-ray photoelectron spectroscopy (XPS) was used for detailed analysis of surface chemistry and, coupled with argon ion sputtering, to map the distribution of elements (with the exception of hydrogen) through the implanted surface. Secondary ion mass spectrometry (SIMS) was also used to examine the distribution of the implanted Ca ions as a function of depth into the Ti substrate. In order to separate the specific effects related to Ca implantation from those inherent to the implantation process itself, ion implantation of Ti, O and Ar was also examined.

2. Experimental

Commercial purity (cp) grade 1 Ti discs (Goodfellow Cambridge Ltd., Cambridge, UK) were polished to a mirror finish using 1200 and 2400 grit SiC paper followed by 0.1 μm colloidal silica suspension plus 30% H_2O_2 (10%, v/v). Cleaning was then performed by ultra-sonication in acetone, methanol and ultra-pure water (UPW) for 5 min, respectively. Samples were dried under a stream of compressed air and stored in Al foil in a desiccator until use. Analyses were performed on polished titanium as a control (cp Ti), Ca ion implanted Ti (Ca–Ti) and Ca–Ti following immersion in ultra-pure water. In order to discriminate between the physical effects of the implantation process and the chemical changes due to Ca implantation, similar experiments were also carried out on oxygen implanted Ti (O–Ti), titanium implanted Ti (Ti–Ti) and argon implanted Ti (Ar–Ti).

Ion implantation was carried out (Department of Electrical and Electronic Engineering, Imperial College of Science, Technology and Medicine, London) using $^{40}Ca^+$ ions at a dose of 1×10^{17} ions cm^{-2} using an implantation energy of 40 keV. O, Ti and Ar ions were implanted at the same dose and the implantation parameters were adjusted in order to obtain similar surface concentrations of the implanted ions; O implantation was performed using $^{16}O_2^+$ ions at 20 keV (equivalent to O^+ at 10 keV), Ti implantation using $^{48}Ti^+$ at 50 keV and Ar implantation using $^{40}Ar^+$ at 40 keV. Following implantation, samples were wrapped in aluminium foil and stored in a desiccator. Immersion experiments were carried out in a sealed plastic container with the sample face upwards in 5 ml ultra-pure water for 18 h at room temperature. Samples were blown dry with compressed air following immersion and analysed immediately.

Computer simulations using the Profile Code software [20] were carried out to predict the ion range and depth profiles of the implanted ions in the Ti target. A second (Monte Carlo) simulation program, SRIM [21], was used to estimate the degree of disturbance to the host Ti lattice by the incident ions. This is described by a parameter known as the displacements per atom (dpa), which may be interpreted as the number of times that any lattice atom is involved in a collision in which the energy is greater than the lattice energy. Samples are generally amorphous, as assessed by X-ray diffraction, if the dpa exceeds 0.1, i.e. if one atom in every 10 has been displaced.

XPS (ESCALAB 220i XL, Thermo Electron Corporation, East Grinstead, UK) was used to determine the chemical composition of the surfaces. Survey spectra were obtained using a pass energy of 100 eV, with high resolution regions acquired at 20 eV pass energy. Elemental profiles were recorded by etching the surface of the sample with an Ar^+ ion beam at 6 keV. The etch current was maintained at 0.4 μA throughout the experiments. XPS survey and region data were recorded for up to 26 levels at times of up to 11,470 s (3.19 h). Acquisition was halted once the O to Ti ratio became less than 0.1. The pressure in the chamber was maintained at 1×10^{-7} mbar by controlling the inflow of Ar (base pressure $<1 \times 10^{-9}$ mbar). XPS data were quantified using Shirley background subtraction and Wagner sensitivity factors. As no Ar was observed on any of the surfaces prior to etching it was excluded from the quantifications.

XPS depth profiles are generally calibrated by etching standards of known thickness, commonly SiO_2. This approach was not adopted in the current work, since the etch rate of Ti

metal is likely to be significantly different from that of SiO_2. Instead, an attempt was made to convert the profiles from a function of etch time into a function of depth by measuring the depths of the etched craters using a white light interferometer (Zygo-New View 200). However, the etch pits were very shallow and the calibration was severely hampered by the difference in etch rates of the Ti metal and oxidised Ti and variations in the oxide layer thickness on implanted and non-implanted samples. From a non-implanted Ti sample, very approximate etch rates of 24 and 49 nm h^{-1} were obtained for Ti and oxidised Ti, respectively. Given the high degree of error in these values, and the fact that implantation of Ca is likely to affect the etch rates, the profiles in the current work are presented as a function of etch time.

SIMS was conducted using an Atomika 6500 ion microprobe (Perkin-Elmer) with an O_2^+ primary ion beam (3 mA, 8 kV) of beam width 50 μm and analysis area 200 μm × 200 μm at normal incidence. An O_2^+ primary ion beam has the advantage of enhancing secondary ion yields whilst avoiding artefacts associated with the interface between the Ti oxide and the underlying metal, since the sputtered material is always oxidised Ti. All mass channels recorded were normalised to the Ti^+ secondary ion intensity associated with the Ti metal at the last data point in the depth profile, and the spectra scaled to give an arbitrary Ti intensity of 10^6 at this end point.

An approximate sputter rate was estimated by measuring the SIMS crater depth from a standard cp Ti sample using a white light interferometer (Zygo-New View 200), with a 10× Mirau objective. This offers a magnification of 200, resulting in a field of view area of 0.70 mm × 0.53 mm and lateral resolution of 1.18 μm. It would be misleading to assume that Ti metal and the native oxide surface layer have the same sputter rate, and Ca ion implantation may affect the sputter rate even further. While the use of an O_2^+ primary ion beam will minimise variations, it must be emphasised that the sputter rate of 0.44 μm h^{-1} used to calibrate the depth profiles is an approximate value only.

3. Results and discussion

Fig. 1 compares the Profile Code simulation for implantation of Ca into Ti with the depth profile of the implanted Ca ions measured using SIMS. The two distributions are very similar in appearance, showing a peak in Ca at ~200 Å depth and a tailing off at ~600 Å, although the Ca distribution from SIMS is slightly narrower and the tail slightly longer than in the simulation.

The XPS profile (as a function of etch time) in Fig. 2a shows some additional features. Firstly, a peak in the relative Ca concentration can be seen at the surface which is not observed in the SIMS profile. One limitation of the dynamic SIMS experiment is that in the first few nanometres (the pre-equilibrium period), both the ion yields and sputter yields are changing. Coupled with the higher etch rate, this means that in the very near surface region, XPS probably presents a more accurate picture of the chemistry. The development of ultra-low energy SIMS profiling with sub-nm depth resolutions will allow

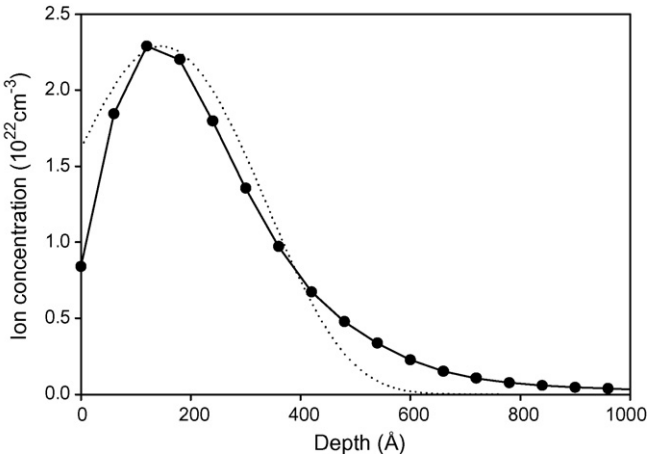

Fig. 1. Depth profiles for implantation of 1×10^{17} ions cm^{-2} $^{40}Ca^+$ into Ti at 40 keV. Dotted lines show the simulation, using Profile Code software, of Ca concentration as a function of depth. Solid lines show the $^{40}Ca^+$ secondary ion signal as a function of depth measured using secondary ion mass spectrometry. The maximum secondary ion signal has been normalised to the peak in the simulated concentration profile.

us in future work to confirm the XPS results. The Ca 2p core level spectrum from the un-etched surface showed a simple spin orbit doublet (Fig. 2b(i), $t = 0$ min), with a Ca $2p_{3/2}$ binding energy of 347.5 eV, which is probably largely attributable to CaO (E_B = 347.1 eV [22]), although the presence of $CaTiO_3$ is not ruled out (E_B = 346.9 eV [23]). The surface Ca/Ti ratio was 0.20. This decreased on etching to a minimum of 0.09 at ~3 min, accompanied by a broadening of the Ca 2p peaks (Fig. 2b), and then increased, showing two deeper lying Ca/Ti maxima at etch times of ~17 and 29 min. At these later times the Ca/Ti ratio was found to be higher than at the immediate surface (Ca/Ti = 0.23 and 0.21, respectively), while the 2p peaks showed further broadening, with a shoulder to low binding energy possibly indicating the presence of Ca in the metallic state (E_B = 345.7 eV [22]).

It is interesting to note that Ikeyama et al. [10,11] saw a double Ca peak in the SIMS depth profile of as-implanted Ca–Ti (3×10^{17} ions cm^{-2}, 35 keV) which they attributed to migration of Ca towards the surface. They also saw a thickening of the oxide layer. These investigators used a 9.8 keV Ar^+ primary ion beam for analysis and it is possible that the double-peak feature is related in part to changes in the secondary ion yields and sputter rates across the metal-oxide interface. Such changes are minimised by using an O_2^+ primary ion beam for SIMS analysis, since the surface being sputtered is always oxidised.

Following immersion for 18 h in ultra-pure water, the Ca/Ti profile as a function of etch time was found to be considerably different (Fig. 2a). Ca levels were dramatically reduced, both at the surface (Ca/Ti = 0.08) and within the bulk Ti (Ca/Ti = 0.05 at 17 and 33 min). The Ca 2p peaks (Fig. 2b), while reduced in relative intensity, were similar in shape and position to those of the as-implanted sample (at $t = 0$ s, E_B = 347.1 eV).

Loss of Ca from both the surface and sub-surface regions on exposure to water has also been seen in SIMS depth profiles (Fig. 3). After 24 h immersion there was a large reduction in

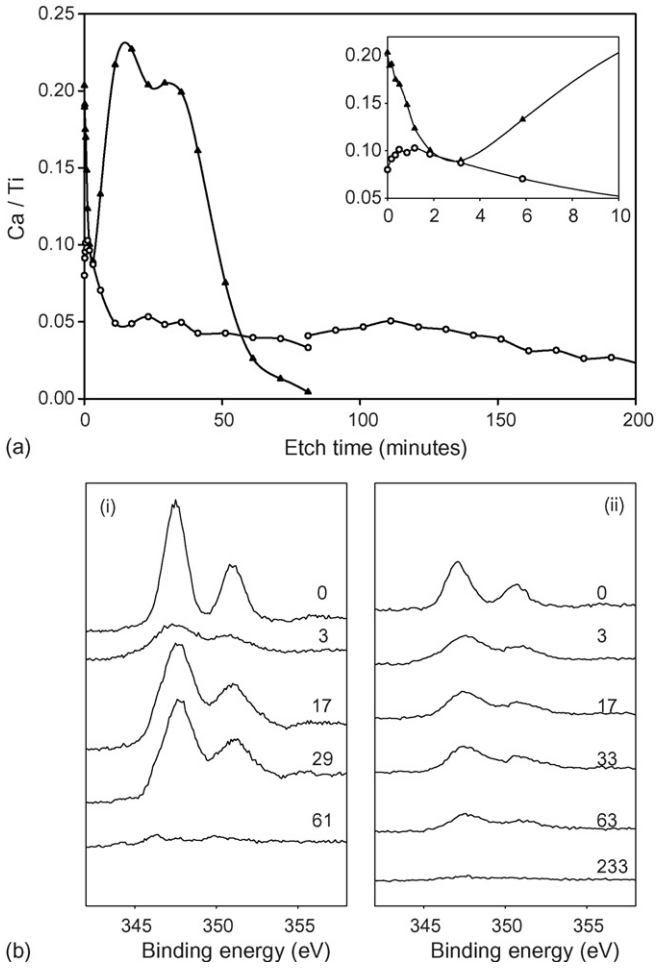

Fig. 2. XPS analysis of Ca 2p peaks as a function of depth for Ca–Ti. (a) Ca/Ti ratios plotted as a function of etch time. Solid triangles denote the as-implanted Ca–Ti sample and open circles the Ca–Ti sample following 18 h immersion in ultra-pure water. The inset shows the variation in Ca/Ti ratios in the near surface region. All lines have been spline-smoothed as a guide to the eye. (b) Ca 2p core level XPS peaks at various etch times: (i) in the as-implanted Ca–Ti sample and (ii) following 18 h immersion in ultra-pure water. The etch time to the nearest minute is shown on the spectra. The spectra have been normalised to the area of the corresponding Ti 2p peak.

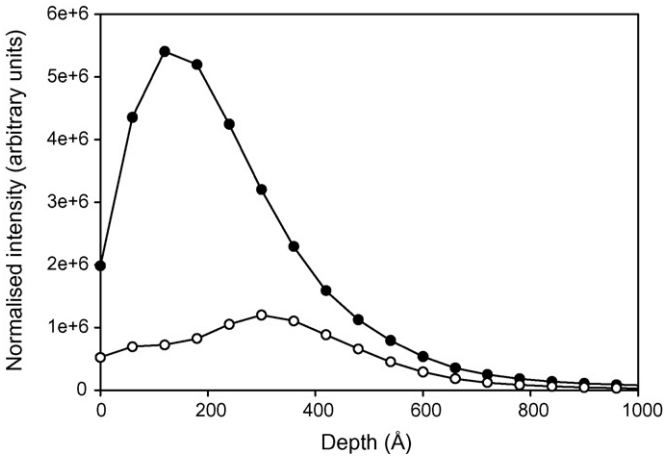

Fig. 3. Ca depth profiles measured using SIMS for ion implanted Ca–Ti implanted in a different batch, but to the same dose and at the same energy, before (solid circles) and after (open circles) immersion in ultra-pure water for 24 h.

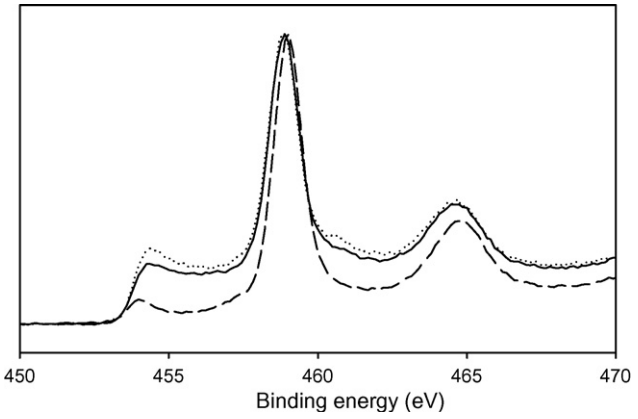

Fig. 4. Ti 2p peaks at the surface for cp Ti (dashed line), Ca–Ti before (dotted line) and Ca–Ti after (solid line) immersion in water for 18 h. The spectra have been normalised to the peak height maximum.

$^{40}Ca^{+}$ secondary ion intensity throughout the implanted region, with the maximum signal reduced by a factor of about 5 and the position of the maximum shifted to ~300 Å. SIMS has the advantage of a much lower detection limit than XPS, allowing the analysis of very low concentrations of implanted ions [24].

Following immersion in water, the surfaces of the Ca–Ti samples examined in this study turned a deep blue colour (see below). Such a phenomenon may be associated with oxidation of the surface, the colour arising due to an interference effect. Light reflected from the air-oxide and oxide-metal interfaces interferes constructively for certain wavelengths and destructively for others, depending on the thickness and refractive index of the transparent oxide layer. In a study of anodically formed oxide layers on Ti, a blue colour was observed for oxide thicknesses of ~70–100 nm [25]. Alternatively, blue colouration can result from the presence of Ti in reduced oxidation states [26].

Oxide layer thicknesses and oxidation states can be assessed by examining the shape of the Ti 2p core level spectrum. In polished cp Ti (Fig. 4), this is dominated by the contribution from the Ti^{4+} cations in the TiO_2-like surface layer, with major peaks at binding energies of 459.0 and 464.9 eV, similar to those of rutile (Ti $2p_{3/2}$ E_B = 458.8 eV; Ti $2p_{1/2}$ E_B = 464.5 eV [27]). Provided that the thickness of the oxide layer is less than the sampling depth of XPS (~100 Å for $h\nu$ = 1486.6 eV), a $2p_{3/2}$ contribution from the underlying Ti^0 metal is readily resolved as a reasonably sharp feature to lower binding energy at 454.0 eV, in good agreement with the published value [27]. If the oxide layer thickness increases, this peak will decrease in relative intensity. The low intensity between the Ti^0 and Ti^{4+} $2p_{3/2}$ peaks corresponds to photoelectrons originating from Ti^{2+} and Ti^{3+}.

The Ti 2p spectrum from the Ca–Ti sample prior to immersion in water was similar to that of cp Ti (Fig. 4), but did not show the sharp peak due to Ti metal at lower binding energy.

Instead, a broad region of higher intensity relative to the Ti^{4+} $2p_{3/2}$ peak extended downwards in binding energy, with a shallow peak at 454.4 eV. The intensity in this region contained contributions from Ti^{2+} (E_B TiO = 455.1 eV [28]) and Ti^{3+} (E_B Ti_2O_3 = 457.5 eV [28]), as well as titanium carbide (E_B = 454.6 eV [29]) formed during the ion implantation process. Any peak due to the underlying Ti metal could not be resolved. The Ti^{4+} $2p_{3/2}$ maximum appeared at a very slightly lower binding energy than that of the non-implanted sample (458.8 eV). The Ti $2p_{3/2}$ binding energy of $CaTiO_3$ has been reported as 458.6 eV [23] and 458.9 eV [30], making a distinction from TiO_2 (E_B = 458.8 eV [27]) impossible with the instrument used. The presence of other phases such as $Ca_4Ti_3O_{10}$ may make accurate determination of the exact constituent components impossible even using ultra-high resolution XPS.

Following immersion in water for 18 h, the Ti 2p peak shape remained very similar (Fig. 4). The "Ti^{n+}" ($n < 4$) components to low binding energy of the Ti^{4+} peaks were slightly reduced in intensity. This suggests that the blue colouration of the sample was due to surface oxidation, rather than oxide reduction. However, growth of the surface oxide layer to a sufficient thickness to give the deep blue colour observed would be expected to result in a considerably greater reduction in the intensity of the Ti^{n+} components. In order to fully understand the processes occurring, it was therefore necessary to examine the accompanying changes in oxygen and carbon as a function of depth into the sample.

Since SIMS was carried out using an O_2^+ primary beam, it was not possible to use this technique to follow the distribution of oxygen within the Ti. Using XPS, however, the variation in the O/Ti ratio for the as-implanted Ca–Ti sample was found to be reasonably similar to that of a non-implanted cp Ti sample, showing a rapid decay in oxygen signal with etch time (Fig. 5). The concentration of oxygen was a little lower than that of the non-implanted material close to the surface, but fell less rapidly and so extended further into the sample. Detailed examination of the depth profile revealed that a small shoulder had formed in the oxygen profile at ~10 min etch time. It is notable that the point of inflection of the O/Ti distribution occurred just below the Ca/Ti minimum and that the shoulder correlated with a rise in Ca/Ti ratio, with oxygen present throughout the Ca implanted region.

Several studies exist in the literature which show depth profiles following single-ion implantation of Ca into Ti [4,9,19,31] or Ti alloys [31,32]. For relatively low implantation energies, as in this work, O was detected across the entire depth of implantation, with the specific shape of the distribution depending on the implantation parameters employed [9,32]. This was attributed to oxidation either during or after implantation, but it was not possible to determine which [31]. However, simulations have shown previously [6] that the native Ti oxide layer is fully sputtered away during the ion implantation process and that implantation occurs into the metal. In view of the low partial pressures of oxygen available in the implanter, therefore, it seems unlikely that oxidation to the depths involved occurred during the implantation process. This will be discussed further below.

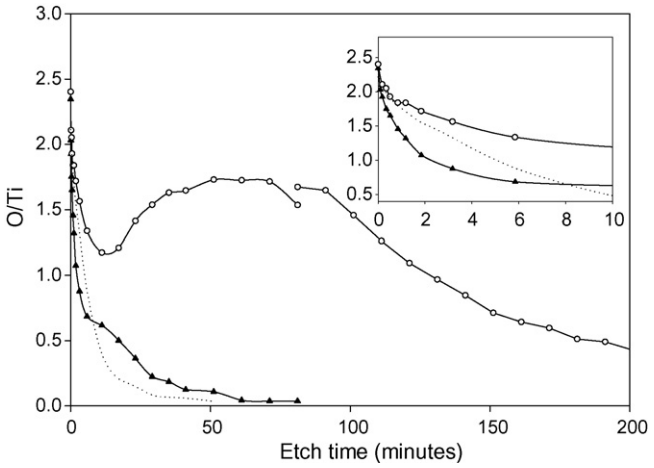

Fig. 5. XPS O/Ti ratios vs. etch time for Ca implanted Ti surfaces. Solid triangles denote the as-implanted Ca–Ti sample and open circles the Ca–Ti sample following 18 h immersion in ultra-pure water. The abrupt rise in the profile from the immersed sample at ~80 min etching was due to continuation of the experiment following an overnight break during which the surface re-oxidised. For comparison, the variation in the O/Ti ratio of a non-implanted cp Ti sample is shown as a dotted line. The inset shows the variation in Ca/Ti ratios in the near surface region. All lines have been spline-smoothed as a guide to the eye.

Immersion of the Ca–Ti sample in water for 18 h resulted in a very different oxygen profile (Fig. 5). Initially the rate of decrease of the O/Ti ratio was similar to that in the control sample. However, the oxygen levels remained higher than in the other samples. For etch times above 10 min the oxygen concentration rapidly rose, showing a broad maximum after ~70 min etching. The presence of a large amount of sub-surface oxygen following immersion suggests that the passive nature of the native Ti surface was compromised by the implantation of Ca.

The resulting thickened oxide layer would explain the blue colouration of the immersed sample. However, it remained unclear why this thickened layer could not be identified in the Ti 2p spectrum from the un-etched surface (Fig. 4), nor why there was a large drop in the O/Ti ratio after ~10 min etching; the same time at which there was a shoulder in the as-implanted sample before immersion. In order to address these questions it was necessary to examine the C 1s spectrum. Carbon was found both at the surface and in the sub-surface regions (Fig. 6a). The surface levels were dominated by the hydrocarbon contamination typical of Ti surfaces [27], but also displayed a small peak attributable to carbide species (carbide/Ti ratio = 0.11) at ~282 eV. This is in contrast to Ca implanted Ti analysed by Hanawa et al. (18 keV, 10^{22} ions m^{-2}), where no carbide was detected [31]. On etching, the hydrocarbon contamination peak rapidly diminished in magnitude, while the relative carbide concentration increased initially, showing a maximum at ~3.2 min (Fig. 6b). This peak occurred at around the same depth as the first point of inflection on the O/Ti curve and just below the minimum in the Ca/Ti ratio. Since the native oxide layer on the cp Ti surface is fully sputtered away during Ca ion

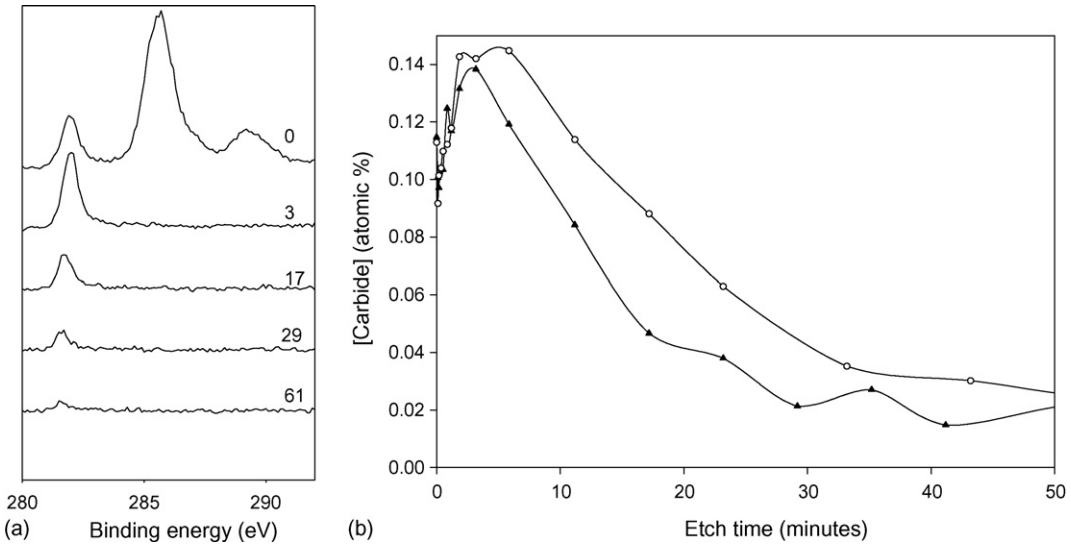

Fig. 6. XPS analysis of C 1s peaks as a function of depth. (a) C 1s spectra from the as-implanted Ca–Ti sample after the same etch times as Fig. 2. (b) Atomic percentage carbide as a function of etch time. Solid triangles denote the as-implanted Ca–Ti sample and open circles the Ca–Ti sample following 18 h immersion in ultra-pure water. All lines have been spline-smoothed as a guide to the eye.

implantation under the conditions used in this work [6], it is possible that the highly reactive Ti surface exposed may react with residual hydrocarbons in the implantation chamber to form carbide species. Additionally, the energetic ion implantation process may lead to some recoil implantation of adsorbed contaminant carbon into the Ti surface. The depth profiles (Fig. 6b) indicate that the carbide was primarily located a little way beneath the surface.

Immersion in water for 18 h did not dramatically alter the distribution of carbide (Fig. 6b). The presence of the sub-surface carbide explains the drop in O/Ti ratio beneath the surface. Since the Ti 2p peak shape was little altered on immersion, it can be further deduced that there was no significant increase in the thickness of the oxide layer above the carbide layer. The Ca-modified Ti below the carbide layer was readily oxidised, but was too deep to contribute significantly to the Ti 2p peak shape.

This is illustrated further in Fig. 7, which shows the overlaid high resolution Ti 2p region data for control cp Ti, single crystal rutile and Ca–Ti before and after immersion in water. Cp Ti, on etching (Fig. 7a), initially showed an increase in intensity in the Ti^{3+} region, followed by Ti^{2+} and eventually Ti^{0} metal which, as expected, dominated the spectrum in the later stages of etching. For comparison, single crystal rutile TiO_2 (Fig. 7b) showed a similar increase in Ti^{3+} followed by Ti^{2+}-like components, but did not show a fully reduced metallic component even after prolonged etching. The major difference in the spectrum from Ca–Ti (Fig. 7c) compared to that from cp Ti was the clear increase in the carbide component, at a binding energy (E_B = 454.6 eV) markedly higher than that of the Ti^{0} peaks, in the earlier stages of etching. While the immersed Ca–Ti sample retained this feature (Fig. 7d), it additionally exhibited the development of the deeper lying oxidised layer. In the intermediate stages of etching, the peak shapes resembled those of the etched single crystal rutile sample, prior to the emergence of the Ti^{0} metal peaks on still further etching.

Compromised passivity of the surface would also explain the presence of oxygen across the implanted region in as-implanted Ca–Ti samples. Following implantation, with its inherent sputtering of the native Ti oxide, the surface re-oxidises on

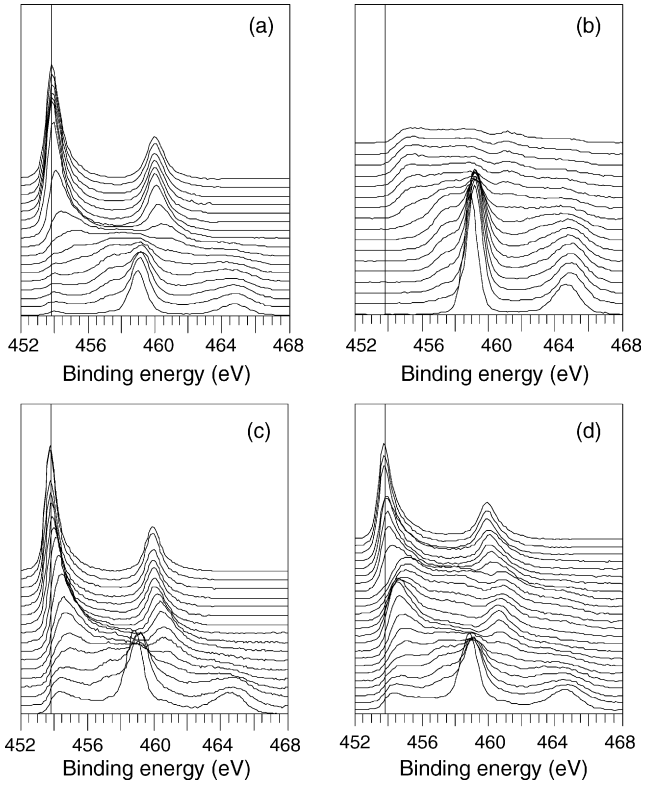

Fig. 7. Overlaid Ti 2p region data from XPS depth profiles: (a) control cp Ti polished surface, (b) TiO_2 rutile single crystal, (c) Ca–Ti surface (as-implanted), and (d) Ca–Ti surface (after 18 h in UPW). Spectra are shown at the following etch times: (a)–(c) 0, 5, 10, 20, 30, 50, 70, 110, 190, 350, 670, 1030, 1390, 2110, 2470, 3670 and 4870 s (total etch time 81 min 10 s); (d) 0, 5, 10, 20, 30, 50, 70, 110, 190, 350, 670, 1030, 1390, 1990, 2530, 3790, 6190, 6790, 7390, 7991, 8591 and 9191 s (total etch time 153 min 11 s).

removal to air. This re-oxidation occurs both above and below the maximum carbide concentration, the presence of Ca allowing greater oxygen diffusion into Ca–Ti than occurs for bare cp Ti, where the passive oxide forms very quickly, preventing further diffusion and oxide thickening. The oxidation of Ca–Ti in the presence of water appears to be massively accelerated by the accompanying release of Ca ions into solution.

In order to determine whether the surface reactivity was due specifically to the implantation of calcium, or whether it was a consequence of the ion implantation process, Ti samples were implanted with Ti^+, O^+ and Ar^+ ions. Aside from the presence of Ar, the surface chemistry of the Ar–Ti sample was very similar to that of Ti–Ti. Analysis of both samples showed the presence of carbide in addition to hydrocarbon contamination and depth profiling demonstrated that the relative concentration of carbide again increased on initial Ar^+ etching. The Ti 2p peak shapes of the two samples were very similar (Fig. 8a), confirming the presence of titanium carbide as well as reduced oxide species, although both showed reduced intensity relative to Ti^{4+} compared to Ca–Ti. This suggests that the presence of both titanium carbide and the reduced oxides is indeed a result of the implantation process itself and not limited to the implantation of Ca. Implantation of oxygen, on the other hand, resulted in no carbide formation, and a reduced relative intensity of Ti sub-oxide species at the surface (Fig. 8a). It is likely that the reactive oxygen ion beam rapidly oxidises hydrocarbon contamination at the surface to volatile species such as CO_2 rather than allowing transfer of energy with consequent C implantation and reaction. Similarly, the rapid reaction of the sputtered Ti surface resulted in a more fully oxidised interface than the relatively slower oxidation process occurring on removal of the other samples from the ion implanter, also potentially reducing the formation of titanium carbide.

The similarity of Ar–Ti and Ti–Ti extended to the depth profiles. Fig. 8b shows almost identical O/Ti distributions as a function of etch time. The O/Ti ratios were slightly elevated compared to both cp Ti and Ca–Ti (Fig. 5), but did not show the shoulder apparent in Ca–Ti. As expected the O–Ti sample showed significantly greater levels of oxygen throughout the profile. Immersion of the Ar, Ti and O implanted samples in water for 18 h produced no significant change in the depth profile, indicating that these surfaces were stable.

These results indicate that neither the presence of increased levels of titanium sub-oxide species, nor the sub-surface carbide were directly responsible for the increased susceptibility to oxidation of the Ca implanted surface. However, it is possible that damage created during the implantation process itself might be a factor. Damage per atom (dpa) profiles generated from SRIM simulations showed deeper lying damage maxima with a larger dpa value for implanted Ca than for the other ions (data not shown). The relative dpa maxima were 18, 17, 7 and 1 for Ca, Ar, Ti and O, respectively. However, the assumptions made for setting up SRIM are inexact and the values obtained could be an order of magnitude wrong. Since all the dpa values were very much greater than 0.1, it is reasonable to assume that all the implanted surfaces were amorphous. It appears that it is the chemical nature of the implanted Ca ions and not simply the physical implantation processes that is responsible for the instability of the oxide on the Ca–Ti surface.

One possibility is that the Ca reacts with the damaged Ti lattice to sit in substitutional sites. On exposure to air, the mobile Ca reacts with oxygen and water in the atmosphere, forming CaO and $Ca(OH)_2$ within the implanted layer. In the aqueous environment, the oxidation and hydrolysis progresses faster. The formation of slightly soluble $Ca(OH)_2$, and its subsequent dissolution may result in defects in the surface film, enabling further oxidation, hydroxylation and dissolution of Ca and allowing oxygen to penetrate to sub-surface layers. It remains unclear at present whether Ti cations are released into solution alongside Ca. When Ti is implanted, it is possible that lattice substitution results in a largely ‘‘healed’’ surface, which

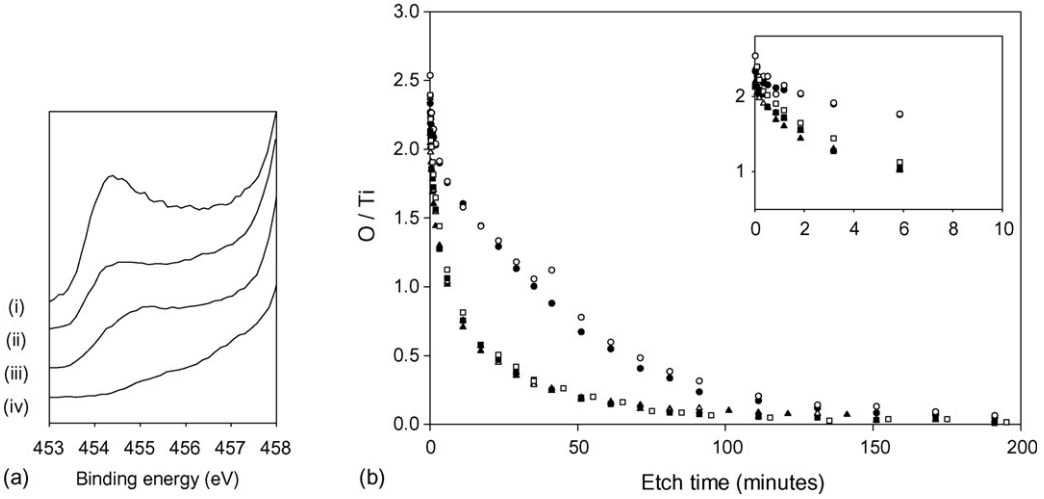

Fig. 8. (a) Photoelectron intensity in the Ti $2p_{3/2}$ core level region below the Ti^{4+} peaks for Ti samples implanted with (i) Ca, (ii) Ti, (iii) Ar and (iv) O ions. (b) XPS O/Ti ratios as a function of etch time for Ti implanted with Ti (triangles), O (circles) and Ar (squares) both before (solid symbols) and after (open symbols) immersion in water for 18 h.

behaves similarly to non-implanted Ti, oxidising rapidly in air to form a passive layer that is impervious to further oxidation in air water. Implantation with O may also result in lattice substitution, but the implanted ions are essentially stable, so that any further oxidation in air or water is again restricted to the immediate surface. Chemically inert Ar may not substitute for lattice sites at all, but sit interstitially; again, the surface behaves like non-implanted Ti on exposure to air and water.

It is remarkable that this oxidation in solution has not been reported previously. One possible reason is the transient nature of the effects. The corrosion experiments by Krupa et al., for example, showed only pitting in Ca implanted Ti at high levels of anodic polarisation (>2.5 V) [4,12]. However, the test samples were allowed to equilibrate for at least 13 h prior to testing. This would enable time for Ca release and oxide thickening prior to testing. Furthermore, these experiments were carried out in simulated body fluids, where the presence of other ions in solution is likely to have a major influence on the surface chemistry. SIMS depth distributions from Ca–Ti [4] and Ti co-implanted with Ca and P [33] were reported to show an increase in Ca, O and P following 3000 h immersion, indicating the formation of calcium phosphate precipitates on the surface.

However, a more recent study which examined the electrochemical behaviour of Ca implanted Ti (15 and 20 keV, 5×10^{16} ions cm^{-2}) in Hank's solution largely supported the current work [13]. Up to 2000 s immersion time, the open-circuit potential of the Ca–Ti sample showed numerous fluctuations attributed to Ca dissolution and precipitation of Ca-containing compounds. Furthermore, cyclic voltammetry indicated that, unlike cp Ti, the surface was not fully covered with a protective oxide film.

No depth profiles exist in the literature for Ca implanted Ti following immersion in pure water. Immersion of Ca–Ti (18 keV, 10^{17} ions cm^{-2}) in nitric acid and phosphate-citric acid buffer resulted primarily in dissolution of the outermost oxide layers. This gave a drop in Ca concentration at the surface, but no accompanying increase in oxygen concentration within the samples [19]. Ca ion loss from Ca–Ti [14] and Ti co-implanted with Ca and P [16] has also been observed on immersion in simple NaCl solutions. However, the depth distributions of the elements were not examined.

Of course it is possible that the implantation parameters are important. The beam energy in the current work was 40 keV, while Krupa et al. used a beam energy of 25 keV [4,12] and Hanawa et al. 18 keV [18,19]. Different beam energies (and different ion doses) will result in different distributions of Ca ions within the Ti and quite possibly different surface reactivities. Indeed, in response to Howlett [34], Hanawa argue that Ti implanted at 18 keV will behave very differently to Ti implanted at 200 keV [35] and would take ~60,000 years to release all the calcium into phosphate buffer at pH 7.4. It is also possible that the length and conditions of storage of the samples following implantation is important. The Ca–Ti immersion described in the current work was carried out less than 2 months after implantation. However, it must be noted that when Ca–Ti samples from the same implantation batch were immersed in water 6 months after implantation, they did not all turn fully blue across the surface. Some samples displayed patches of silver and a few remained fully silver. Samples that remained silver were analysed and found to show a drop in Ca at the immediate surface almost identical to the blue samples, but no reduction in Ca concentrations deeper within the Ti and no accompanying increase in O concentrations. The reasons for this remain unclear at present, but it is possible that the surface partially or wholly repassivates over time.

Notably, however, similar effects to those obtained in the current work *do* appear to have been observed for Ti implanted with Na (18–22 keV, 8×10^{16} to 4×10^{17} ions cm^{-2}) [36–38]. These studies show depth profiles in which the O concentration of the as-implanted Na–Ti samples follows the distribution of the Na concentration. Following immersion in water, the depth profiles repeatedly showed loss of sodium ions from the implanted region of the surface and elevated oxygen concentrations to a greater depth than in the as-implanted samples. However, the authors commented in the text that the oxygen distribution ''remains unchanged'' and no mention was made of any changes in sample colour. In another study by the same group [39], Na–Ti samples (20 keV, 3.2×10^{17} ions cm^{-2}) hydrolysed in deionised water showed both loss of sodium from the surface and significantly higher levels of hydroxylation (H concentration) than untreated Ti control surfaces, on which there was a negligible increase in hydroxyl levels even after 120 h in deionised water.

This similarity in behaviour is important, because Na–Ti has been shown to enhance the rate of hydroxyapatite-like calcium phosphate formation at the surface from simulated body fluids [36–43] in a similar manner to Ca–Ti [4,14]. The variation in surface chemistry with time is particularly significant because it may influence biological response to the ion implanted surfaces. The surface chemistry change may be the reason why Ca implanted Ti inhibited the initial adhesion of cells, while further exposure to the surface resulted in increased cell proliferation [5,6]. Interpretation of any results based on Ca implanted samples must consider carefully the changing surface composition of the material.

4. Conclusions

XPS depth profiling has been used to show that the passive oxide film formed on Ti can be compromised by calcium ion implantation. After 18 h in ultra-pure water the implanted Ca levels fell and sub-surface oxygen proportions rose considerably. SIMS confirmed the loss of sub-surface calcium. Comparisons with Ti implanted with other ions suggested that the sub-surface oxidation was not a consequence of the implantation process, but a result of the Ca dissolution from the oxide. This is likely to have implications for cells and tissues in the vicinity of the surface, particularly at very early time-points.

Acknowledgements

This work was partly funded by the EPSRC through the award of a fast stream grant (GR/M85357) and an advanced

fellowship (FHJ-GR/R77582). We also acknowledge the UCL Eastman Dental Institute for the ongoing support of the XPS instrumentation.

References

[1] G. Manivasagam, U.K. Mudali, R. Asokamani, B. Raj, Corr. Rev. 21 (2003) 125–259.
[2] T. Hanawa, Y. Kamiura, S. Yamamoto, T. Kohgo, A. Amemiya, H. Ukai, K. Murakami, K. Asaoka, J. Biomed. Mater. Res. 36 (1997) 131–136.
[3] T. Jinno, S.K. Kirk, S. Morita, V.M. Goldberg, J. Arthroplasty 19 (2004) 102–109.
[4] D. Krupa, J. Baszkiewicz, J.A. Kozubowski, A. Barcz, J.W. Sobczak, A. Biliński, M. Lewandowska-Szumieł, B. Rajchel, Biomaterials 22 (2001) 2139–2151.
[5] S. Nayab, L. Shinawi, J. Hobkirk, T.J. Tate, I. Olsen, F.H. Jones, J. Mater. Sci.: Mater. Med. 14 (2003) 991–997.
[6] S.N. Nayab, F.H. Jones, I. Olsen, J. Biomed. Mater. Res. 69A (2004) 651–657.
[7] S.N. Nayab, F.H. Jones, I. Olsen, Biomaterials 26 (2005) 4717–4727.
[8] T. Hanawa, H. Ukai, K. Murakami, J. Electron Spectrosc. Relat. Phenom. 63 (1993) 347–354.
[9] E. Wieser, I. Tsyganov, W. Matz, H. Reuther, S. Oswald, T. Pham, E. Richter, Surf. Coat. Technol. 111 (1999) 103–109.
[10] M. Ikeyama, S. Nakao, H. Morikawa, Y. Yokogawa, L.S. Wielunski, R.A. Clissold, T. Bell, Colloid Surf. B 19 (2000) 263–268.
[11] M. Ikeyama, S. Nakao, H. Morikawa, Y. Yokogawa, L.S. Wielunski, R.A. Clissold, T. Bell, Surf. Coat. Technol. 128 (2000) 400–403.
[12] D. Krupa, J. Baszkiewicz, J. Kozubowski, A. Barcz, J. Sobczak, A. Bilinski, B. Rajchel, Vacuum 63 (2001) 715–719.
[13] E. Byon, S. Moon, S.-B. Cho, C.-Y. Jeong, Y. Yeong, Y.-T. Sul, Surf. Coat. Technol. 200 (2005) 1018–1021.
[14] M.T. Pham, W. Matz, H. Reuther, E. Richter, G. Steiner, S. Oswald, J. Mater. Sci. Lett. 19 (2000) 443–445.
[15] T. Kokubo, H.M. Kim, M. Kawashita, T. Nakamura, J. Mater. Sci.: Mater. Med. 15 (2004) 99–107.
[16] M.T. Pham, W. Matz, H. Reuther, E. Richter, G. Steiner, S. Oswald, Surf. Coat. Technol. 128 (2000) 313–319.
[17] T. Hanawa, M. Kon, H. Doi, H. Ukai, K. Murakami, H. Hamanaka, K. Asaoka, J. Mater. Sci.: Mater. Med. 9 (1998) 89–92.
[18] T. Hanawa, K. Asami, K. Asaoka, Corr. Sci. 38 (1996) 1579–1594.
[19] T. Hanawa, K. Asami, K. Asaoka, Corr. Sci. 38 (1996) 2061–2067.
[20] PROFILE CODE Implant Sciences Co., MA, USA.
[21] SRIM 2000 J.F. Ziegler IBM-Research, NY, USA.
[22] H. Van Doveren, J.A.T.H. Verhoeven, J. Electron Spectrosc. Relat. Phenom. 21 (1980) 265–273.
[23] S. Kaĉiulis, G. Mattogno, A. Napoli, E. Bemporad, F. Ferrari, A. Montenero, G. Gnappi, J. Electron Spectrosc. Relat. Phenom. 95 (1998) 61–69.
[24] D.S. McPhail, J. Mater. Sci. 41 (2006) 873–903.
[25] Y.-T. Sul, C.B. Johansson, Y. Jeong, T. Albrektsson, Med. Eng. Phys. 23 (2001) 329–346.
[26] J. Pan, D. Thierry, C. Leygraf, J. Biomed. Mater. Res. 30 (1996) 393–402.
[27] J. Lausmaa, J. Electron Spectrosc. Relat. Phenom. 81 (1996) 343–361.
[28] G. Lu, S.L. Bernasek, J. Schwartz, Surf. Sci. 458 (2000) 80–90.
[29] D. Briggs, M.P. Seah (Eds.), Practical Surface Analysis. vol. 1, Auger and X-ray Photoelectron Spectroscopy, 2nd ed., Wiley, Chichester, 1990, p. 493.
[30] J.F. Moulder, W.F. Stickle, P.E. Sobol, K.D. Bomben, Handbook of X-ray Photoelectron Spectroscopy, Phys. Electronics Inc., Eden Prarie, USA, 1995.
[31] T. Hanawa, H. Ukai, K. Murakami, K. Asaoka, Mater. Trans. JIM 36 (1995) 438–444.
[32] I. Tsyganov, E. Wieser, W. Matz, H. Reuther, E. Richter, Surf. Coat. Technol. 158–159 (2002) 318–323.
[33] D. Krupa, J. Baszkiewicz, J.A. Kozubowski, A. Barcz, J.W. Sobczak, A. Biliński, M. Lewandowska-Szumieł, B. Rajchel, Biomaterials 26 (2005) 2847–2856.
[34] C.R. Howlett, J. Biomed. Mater. Res. A 44 (1999) 352.
[35] T. Hanawa, J. Biomed. Mater. Res. 44 (1999) 352–353.
[36] M.T. Pham, M.F. Maitz, W. Matz, H. Reuther, E. Richter, G. Steiner, Thin Solid Films 379 (2000) 50–56.
[37] M.T. Pham, W. Matz, D. Grambole, F. Herrmann, H. Reuther, E. Richter, G. Steiner, J. Biomed. Mater. Res. 59 (2002) 716–724.
[38] M.F. Maitz, M.T. Pham, W. Matz, H. Reuther, G. Steiner, Surf. Coat. Technol. 158 (2002) 151–156.
[39] M.T. Pham, M.F. Maitz, D. Grambole, F. Herrmann, H. Reuther, E. Richter, J. Mater. Sci. Lett. 20 (2001) 295–296.
[40] M.T. Pham, W. Matz, H. Reuther, E. Richter, G. Steiner, J. Mater. Sci. Lett. 19 (2000) 1029–1031.
[41] M.F. Maitz, M.T. Pham, W. Matz, H. Reuther, G. Steiner, E. Richter, Biomol. Eng. 19 (2002) 269–272.
[42] D. Krupa, J. Baszkiewicz, B. Rajchel, A. Barcz, J.W. Sobczak, A. Biliński, Vacuum 78 (2005) 161–166.
[43] D. Krupa, J. Baszkiewicz, J.A. Kozubowski, J. Mizera, A. Barcz, J.W. Sobczak, A. Biliński, B. Rajchel, Anal. Bioanal. Chem. 381 (2005) 617–625.